Josephson Junction Microscope for Low-Frequency Fluctuators

L. Tian[1,*] and R. W. Simmonds[2,†]

[1]*Department of Applied Physics and E. L. Ginzton Laboratory, Stanford University, Stanford, California 94305, USA*
[2]*National Institute of Standards and Technology, 325 Broadway, Boulder, Colorado 80305-3328, USA*

(Received 9 May 2007; published 26 September 2007)

The high-Q harmonic oscillator mode of a Josephson junction can be used as a novel probe of spurious two-level systems (TLSs) inside the amorphous oxide tunnel barrier of the junction. In particular, we show that spectroscopic transmission measurements of the junction resonator mode can reveal how the coupling magnitude between the junction and the TLSs varies with an external magnetic field applied in the plane of the tunnel barrier. The proposed experiments offer the possibility of clearly resolving the underlying coupling mechanism for these spurious TLSs, an important decoherence source limiting the quality of superconducting quantum devices.

DOI: 10.1103/PhysRevLett.99.137002 PACS numbers: 85.25.Cp, 03.67.Pp, 74.50.+r

Superconducting quantum circuits have been intensively tested in various regimes in the past few years, from superconducting qubits demonstrating long coherence times to superconducting transmission line cavities coherently coupled to a single Cooper-pair box [1–7]. Such circuits are extremely sensitive to very small quanta and defect states and, hence, have the ability to detect individual microwave photons, charged quasiparticles, as well as spurious two-level systems (TLSs) within or near the Josephson junction tunnel barrier [8,9]. In recent experiments [10,11], TLSs were identified through spectroscopic measurements of a superconducting phase qubit appearing as ''gaps'' or ''splittings'' in the energy spectrum.

The TLS defects can be an unwanted source of decoherence for superconducting quantum bits. The low-frequency noise, which has been shown to be a serious source of decoherence for superconducting qubits [12–14], is very probably induced by such amorphous fluctuators inside or near Josephson junctions [15]. Understanding the origin of these spurious TLSs, their coherent quantum behavior, and their connection to the ubiquitous $1/f$ noise is hence a challenge that will be crucial to the future of superconducting quantum devices. The behavior of a distribution of these TLSs was studied theoretically in Refs. [16–18]. Recently, it was proposed that TLSs can be viewed as qubits themselves [19], given their relatively long coherence times. However, the microscopic origin and the coupling mechanism between the TLSs and the junction remain unresolved. Generally considered to be connected to the amorphous nature of the tunnel barrier [20], movement of unrestrained atoms or charges may lead to a number of possible coupling mechanisms. As originally proposed in Ref. [11], fluctuations of the TLS could lead to variations of the junction critical current. Another possibility requires that the TLSs have fluctuating dipole moments which couple to the electric field found within the junction tunnel barrier [10].

Here we present a scheme that can resolve a variety of *microscopic* properties of the TLSs and distinguish between these two suggested coupling mechanisms through the use of an applied magnetic field. Consider a Josephson junction resonator operating as a high-Q nonlinear cavity mode [21], coupling to the TLSs through its canonical phase (or momentum) operator. This forms a cavity QED system with the junction resonator mode as the cavity and the TLSs as the atoms [22,23]. The junction resonator acts as a microscope for studying the behavior of the TLS. We will show that microwave transmission in the junction resonator carries spectroscopic, interaction (coupling), and spatial information of the TLSs. In particular, the junction resonator can resolve the coupling mechanism between a TLS and the junction. When a TLS couples to the junction through the junction *critical current*, the magnitude of the coupling will be strongly modulated by changing the strength of the magnetic field oriented along the plane of the tunnel barrier. On the contrary, if a TLS can couple only through the junction's *electric field*, the magnetic field will have no effect on the magnitude of this coupling. Changes in the coupling magnitude can be observed by measuring the microwave transmission through the junction resonator. To demonstrate this quantitatively, we calculate the transmission and its noise spectrum in the ''bad cavity'' limit [24], where the dissipation of the junction resonator is much faster than that of the TLS. Our calculations show that the resonances and noise spectrum of the transmission strongly depend on the coupling strength, as well as the energy distribution, dynamic, dissipative, and spatial properties, of a chosen TLS.

Magnetic field modulation of the coupling.—The circuit is shown in Fig. 1, where a Josephson junction with the energy E_{J1} together with a superconducting loop forms an RF-SQUID enclosing a bias flux Φ_b. Magnetic field applied along the plane of the tunnel barrier inside the junction [25] results in a flux of $\Phi_1 = \frac{\hbar}{2e}\varphi_1$. At $\Phi_b = 0$, the effective Josephson energy of the circuit can be written as $-E_J \cos(\delta + \varphi_1/2)$, with

$$E_J = E_{J1}\frac{\sin\varphi_1/2}{\varphi_1/2}$$

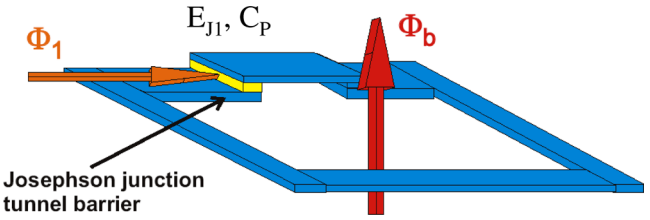

FIG. 1 (color online). Circuit. RF-SQUID loop with in-plane magnetic flux $\Phi_1 = \frac{\hbar}{2e}\varphi_1$, loop flux Φ_b, Josephson energy E_{J1}, and total capacitance C_P.

depending on the magnetic field and δ being the phase difference across the junction. Given a total capacitance C_P (shunt capacitance plus junction capacitance), the junction behaves as an harmonic oscillator of the phase variable δ with the frequency $\omega_c = \sqrt{4e^2 E_J/\hbar^2 C_P}$. Consider a TLS inside the junction with an energy $\hbar\omega_a$ close to $\hbar\omega_c$. When the TLS couples with the critical current of the junction, the coupling can be derived as

$$-E_{J1}\int_0^L dx \cos\left(\delta + \varphi_1 \frac{x}{L}\right)\vec{j}_d \cdot \vec{\sigma} f(x - r_d),$$

where L is the length of the junction along the direction perpendicular to Φ_1, $\vec{j}_d$ describes the polarization and magnitude of the coupling, $\vec{\sigma} = (\sigma_x, \sigma_y, \sigma_z)$ are the Pauli matrices of the TLS, and $f(x - r_d)$ describes the spatial profile of the TLS centered at r_d [15]. For simplicity, we assume $f(x - r_d) = \delta(x - r_d)$ and $\vec{j}_d = (j_x, 0, 0)$, and the coupling becomes $-E_{J1} j_x \cos(\delta + \varphi_1 r_d/L)\sigma_x$. To the lowest order of $(\delta + \varphi_1/2)$, the shifted phase variable, the coupling can be written as $H_c = g_d \sigma_x(\hat{a} + \hat{a}^\dagger)$, with

$$g_d = E_{J1} j_x \sqrt{\frac{2e^2}{C_P \hbar \omega_c}} \sin\varphi_1 \left(\frac{r_d}{L} - \frac{1}{2}\right) \tag{1}$$

and $\hat{a}$ ($\hat{a}^\dagger$) being the annihilation (creation) operator of the phase variable. The coupling hence oscillates with and is strongly affected by the applied flux Φ_1.

In contrast, when the TLS couples to the dielectric field within the Josephson junction, the coupling is $-(2e^2/C_P)(d_0/h_0)(\hat{p}_\delta/\hbar)$, where $\hat{p}_\delta$ is the momentum of the phase variable, d_0 is the size of the dielectric dipole, and h_0 is the thickness of the tunnel barrier. The coupling can be written as $H_c = -ig_c\sigma_x(\hat{a} - \hat{a}^\dagger)$, with

$$g_c = \frac{d_0}{h_0}\sqrt{\frac{e^2\hbar\omega_c}{2C_P}} \tag{2}$$

not depending on the applied magnetic flux Φ_1. Therefore, probing the dependence of the coupling on the magnetic flux will clearly determine which physical mechanism is more visible even if *both* effects are present. Note that the applied magnetic field Φ_1 shifts the frequency of the junction resonator mode, which can be compensated for by adjusting the loop flux Φ_b (see below).

The driving on the junction resonator can be obtained by capacitively coupling the junction to a microwave source with frequency ω_d and amplitude ϵ: $2\epsilon\cos\omega_d t(\hat{a} + \hat{a}^\dagger)$. In the rotating frame, the total Hamiltonian for the coupled TLS and junction resonator is

$$H_t = \Delta_c \hat{a}^\dagger\hat{a} + \frac{\Delta_a}{2}\sigma_z + g(\varphi_1)(\sigma_+\hat{a} + \sigma_-\hat{a}^\dagger) + \epsilon(\hat{a} + \hat{a}^\dagger), \tag{3}$$

with the detunings $\Delta_c = \omega_c - \omega_d$ and $\Delta_a = \omega_a - \omega_d$ and the coupling $g(\varphi_1)$ given by Eq. (1) or Eq. (2) depending on the coupling mechanism. The environmental noise can play a crucial role in the stationary state of the coupled system. Here we treat the noise by the Lindblad form $\kappa\mathcal{L}(\hat{a})\rho + \gamma_d\mathcal{L}(\sigma_-)\rho + \gamma_p\mathcal{L}(\sigma_z)\rho$ in the master equation [26], which includes the dissipation of the junction resonator with rate κ, the decay of the TLS with rate γ_d, and the dephasing of the TLS with rate γ_p.

The model discussed above describes a typical cavity QED system [22,23]. The junction resonator acts as a high-Q cavity driven by microwave source, the TLS acts as a two-level atom, with a Jaynes-Cummings type of coupling between the two. Because of the coupling, the transmission through the junction resonator is imprinted with the information of the TLS. As we will show below, measurement of the microwave transmission provides an effective probe, or a *microscope*, for the TLS. Note that frequencies of the TLSs were observed to be separated by 200 MHz on average [10]. With a coupling magnitude of $g(\varphi_1) \sim 10$ MHz, it is reasonable to assume that only a single TLS satisfies the near-resonance condition $|\omega_a - \omega_c| \sim g$ and affects the transmission in the junction significantly. The other TLSs that are far off-resonance from the junction resonator induce small ac-Stark shifts of the order of $g^2/|\omega_a - \omega_c|$.

Microwave transmission in the junction resonator.—To quantitatively illustrate the effect of the TLS on the transmission in the junction resonator, we study the above system in the bad cavity limit with $\gamma_d, \gamma_p \ll \kappa$; i.e., the dissipation of the junction resonator is much faster than that of the TLS [24]. As a result, the junction resonator mode adiabatically follows the dynamics of the TLS governed by the Bloch equation

$$\frac{d\langle\vec{\sigma}\rangle}{dt} = A_2(\langle\vec{\sigma}\rangle + \vec{B}), \tag{4}$$

with the Pauli matrices $\vec{\sigma} = (\sigma_z, \sigma_+, \sigma_-)^T$. The dynamic matrix is

$$A_2 = \begin{pmatrix} -\gamma_1 & -i\Omega_r^* & i\Omega_r \\ -\frac{i}{2}\Omega_r & i\Delta - \gamma_2 & 0 \\ \frac{i}{2}\Omega_r^* & 0 & -i\Delta - \gamma_2 \end{pmatrix},$$

and the offset vector is $\vec{B} = A_2^{-1}(-\gamma_1, 0, 0)^T$, with

$$\Omega_r = \frac{i2g\epsilon}{\kappa - i\Delta_c}, \tag{5}$$

$$\Delta = \Delta_a - \frac{g^2\Delta_c}{\kappa^2 + \Delta_c^2}, \tag{6}$$

$$\gamma_2 = \frac{\gamma_d}{2} + \gamma_p + \frac{g^2\kappa}{\kappa^2 + \Delta_c^2}, \tag{7}$$

and $\gamma_1 = 2(\gamma_2 - \gamma_p)$ as the dressed parameters. The coupling $g(\varphi_1)$ modifies the dressed detuning Δ and the dressed decoherence rates $\gamma_{1,2}$, and results in a driving Ω_r on the TLS that depends linearly on the coupling. The stationary state of the TLS is $\langle\vec{\sigma}\rangle_{ss} = -\vec{B}$. With $\eta = \Omega_r/(\Delta + i\gamma_2)$, we have $B_z \approx 1 - |\eta|^2\gamma_2/\gamma_1$ and $B_+ = B_-^\star \approx \eta/2$ under the weak driving condition $|\eta| \ll 1$.

Below, we derive the junction transmission defined as $t(\omega_d) = |\kappa\langle\hat{a}\rangle_{ss}/\epsilon|^2$ at the driving frequency ω_d, where the stationary output field is $\langle\hat{a}\rangle_{ss} = (\epsilon + g\langle\sigma_-\rangle_{ss})/(\kappa + i\Delta_c)$. In Fig. 2, we plot the transmission versus the driving frequency at various coupling magnitudes $g(\varphi_1)$. Let $\omega_p^{1,2}$ be the position of the resonance peaks in the transmission spectrum. At $g(\varphi_1) = 0$ with no coupling, a single resonance peak appears at $\omega_d = \omega_c$ and $t(\omega_d) = \kappa^2/(\kappa^2 + \Delta_c^2)$. At $g(\varphi_1) = 10$ MHz, the two resonance peaks appear with a separation of $\omega_p^2 - \omega_p^1 = 38$ MHz. At $g(\varphi_1) = 20$ MHz, the separation of the two resonance peaks increases to $\omega_p^2 - \omega_p^1 = 50$ MHz. To explain this result, we make the following approximation:

$$t(\omega_d) \approx \frac{\kappa^2\Delta_a^2}{(\Delta_a\Delta_c - g^2)^2 + \kappa^2\Delta_a^2} \tag{8}$$

under the condition $\gamma_d, \gamma_p \ll g(\varphi_1), \kappa, |\Delta_a|, |\Delta_c|$, which reveals two resonance peaks satisfying $\Delta_a\Delta_c - g^2 = 0$, i.e., $\omega_p^{(1,2)} = (\omega_a + \omega_c \pm \sqrt{\Delta_{ac}^2 + 4g^2})/2$, respectively, with $\Delta_{ac} = \omega_a - \omega_c$. This shows very good agreement with the curves in Fig. 2. For the coupling given by

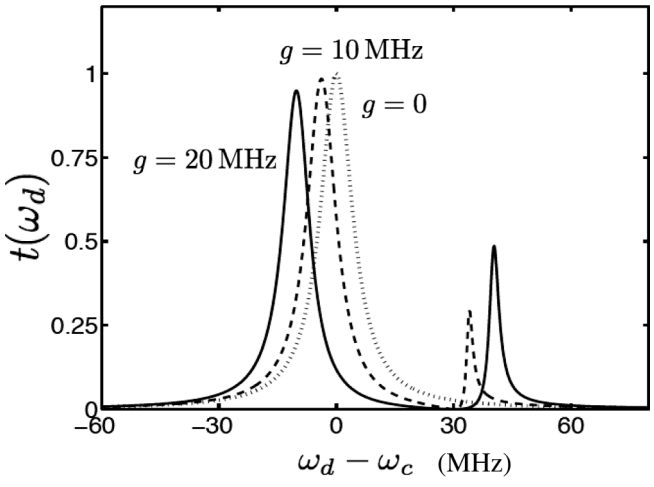

FIG. 2. Transmission spectra with the coupling strength $g = 0$ (dotted curve), $g = 10$ MHz (dashed curve), and $g = 20$ MHz (solid curve). The parameters are $\omega_c = 7$ GHz, $\Delta_{ac} = 30$ MHz, $\gamma_d = 0.2$ MHz, $\gamma_p = 0.1$ MHz, $\kappa = 5$ MHz, and $\epsilon = 1$ MHz for a TLS at the position $r_d = 0.2$.

Eq. (1), adjusting the magnetic flux Φ_1 will thus result in the above change in the transmission spectrum. Note that the transmission reaches a minimum at $\omega_d = \omega_a$ with $t(\omega_a)$ approaching zero, as is shown in Eq. (8). The position of this minimum can be used to determine the frequency of the TLS.

Noise spectrum of the junction transmission.—By measuring the time correlation functions of the transmission spectrum, the noise spectrum of the transmission and, subsequently, the properties of the TLS can be studied. Let $X = (\hat{a} + \hat{a}^\dagger)$ be the linearized operator of the phase variable $(\delta + \varphi_1/2)$. The symmetrized noise spectrum for the operator X can be written as $F_{XX}(\omega) = \int_{-\infty}^{\infty} dt e^{i\omega t}\frac{1}{2} \times \langle X(t)X + XX(t)\rangle - \langle X(t)\rangle\langle X\rangle$. In the bad cavity limit, we have

$$\frac{d}{dt}\hat{a}_\alpha(t) = -(\kappa - i\alpha\Delta_c)\hat{a}_\alpha(t) + \epsilon + g\sigma_\alpha(t), \tag{9}$$

with $\alpha \in \{-, +\}$, $\hat{a}_- = \hat{a}$, and $\hat{a}_+ = \hat{a}^\dagger$, which forms a linear transformation between the Pauli matrices of the TLS and the operators of the junction resonator. The time correlation function $\langle X(t)X\rangle$ [and $\langle XX(t)\rangle$] can then be derived from the time correlation functions of the Pauli matrices.

Following the quantum regression theorem [27], the time correlation functions of the TLS can be derived from Eq. (4). At weak driving with $|\eta| \ll 1$, the matrix A_2 can be approximated to the second order of η ($\eta^\star$) as a diagonal matrix with the elements $\{A_{zz}, A_{++}, A_{--}\}$ (not shown). The time correlation functions can be derived:

$$\langle\sigma_\alpha(t)\sigma_\beta\rangle = e^{A_{\alpha\alpha}t}(\langle\sigma_\alpha\sigma_\beta\rangle - B_\beta B_\alpha) + B_\beta B_\alpha \tag{10}$$

and similarly for $\langle\sigma_\alpha\sigma_\beta(t)\rangle$. Among such time correlation functions, the dominant contribution to $F_{XX}(\omega)$ is from $\langle\sigma_-\sigma_+\rangle \approx 1$.

We consider the normalized noise spectrum $\tilde{F}(\omega) = F_{XX}(\omega)[\kappa^2 + (\omega - \Delta_c)^2]/g^2$, which is directly associated with the parameters of the TLS. It can be calculated that

$$\tilde{F}(\omega) \approx \frac{\gamma_2}{(\omega - \Delta)^2 + \gamma_2^2} + \frac{\gamma_2}{(\omega + \Delta)^2 + \gamma_2^2} \tag{11}$$

to an accuracy of $O(|\eta|^2)$, where the frequencies of the resonance peaks are given by $\omega_{np} = \pm\Delta$ as defined in Eq. (6) and the widths of the resonance peaks are given by γ_2 as defined in Eq. (7). In Fig. 3, we plot $\tilde{F}(\omega)$ and ω_{np} for $g = 20$ MHz over a range of driving frequencies. By measuring the resonances in $\tilde{F}(\omega)$, detailed characterization of the TLS can be achieved. For example, at the driving frequency $\omega_d = \omega_c$ ($\Delta_c = 0$), the position of the resonance peaks is given by $\omega_{np} = \pm\Delta_{ac}$, revealing the frequency of the TLS. At $\Delta_c \neq 0$ but $\Delta_c \sim \kappa$, the position of the resonance peaks strongly depends on the coupling strength g, as is shown in Fig. 3. When reducing the coupling strength to $g \ll \kappa$, the separation of the two resonance peaks linearly depends on the driving frequency and crossing each other at $\Delta_a = 0$.

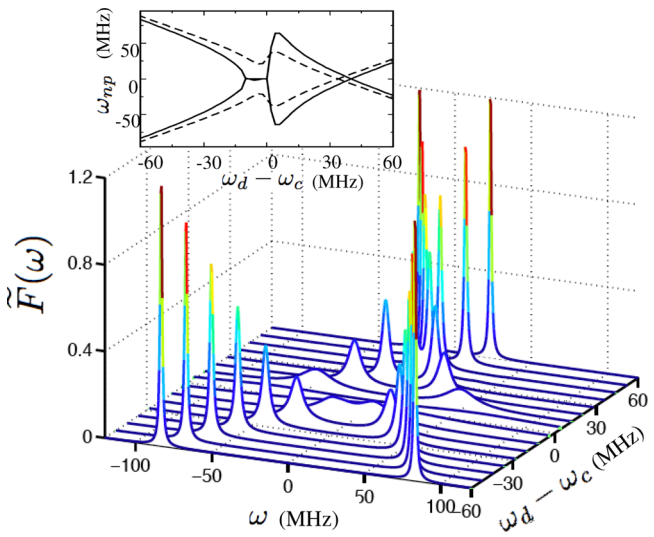

FIG. 3 (color online). Spectrum $\tilde{F}_{\sigma_-\sigma_+}(\omega)$ (main plot) and resonance peaks $\omega_{\rm np}$ (inset) with $g = 20$ MHz and $|\eta| \ll 1$, plotted at various driving frequencies ω_d. For parameters, see the caption in Fig. 2.

Spectroscopic measurements.—The TLSs in the tunnel barrier span a broad range of frequencies. In order to clearly determine the distribution of the coupling and the position of the TLSs, we need to control the resonant frequency of the junction resonator to sweep past individual TLSs in each successive set of transmission measurements. This is achieved by varying the applied magnetic flux Φ_b in the RF-SQUID loop to adjust the total inductance in the RF-SQUID loop. The effective frequency of the junction resonator can be derived as

$$\omega_c = \sqrt{\frac{\cos(2\pi * \Phi_b/\Phi_o)}{L_J C_P} + \frac{1}{L_b C_P}}, \qquad (12)$$

where L_J ($L_J = \hbar^2/4e^2E_J$) is the intrinsic inductance of the Josephson junction when $\Phi_b = 0$, L_b is the self-inductance of the RF-SQUID loop, and C_P is the total capacitance including the shunt capacitance and the junction capacitance. Typical parameters are $L_J = 365$ pH, $L_b = 400$ pH, and $C_P = 2.7$ pF. The frequency of the junction resonator can be tuned from $\omega_c = 7$ GHz at $\Phi_b = 0$ over a large range to well below 1 GHz.

To measure a specific TLS with frequency ω_a, the frequency of the junction resonator ω_c needs to be kept near ω_a throughout the transmission measurements with various flux Φ_1 inside the tunnel barrier. As we discussed previously, ω_c can be shifted when adjusting the flux Φ_1. Here the bias flux Φ_b in the RF-SQUID loop again provides crucial control of the frequency ω_c. By tuning Φ_b, the frequency shift due to Φ_1 can be compensated, and ω_c can stay in a constant energy contour.

Conclusions.—We present a cavity QED scheme for studying the properties of the TLSs in the tunnel barrier of a Josephson junction. The high-Q oscillator mode of the junction resonator acts as a *microscope* for probing the spectral, spatial, and coupling properties of the TLSs by measuring the microwave transmission in the junction. In particular, our study shows that the coupling mechanism between the junction and the TLSs can be determined by applying a magnetic field in the plane of the junction tunnel barrier.

L. T. is supported by the SORST program of the Japan Science of Technology Corporation (JST) and Special Coordination Funds for Promoting Science and Technology of University of Tokyo. R. W. S. is supported by NIST and DTO under Grant No. W911NF-05-R-0009.

*ltian@stanford.edu
†simmonds@boulder.nist.gov

[1] Y. Makhlin, G. Schön, and A. Shnirman, Rev. Mod. Phys. **73**, 357 (2001).
[2] W. D. Oliver *et al.*, Science **310**, 1653 (2005); S. O. Valenzuela *et al.*, Science **314**, 1589 (2006).
[3] I. Chiorescu *et al.*, Nature (London) **431**, 159 (2004); A. Lupascu *et al.*, Nature Phys. **3**, 119 (2007).
[4] R. H. Koch *et al.*, Phys. Rev. Lett. **96**, 127001 (2006).
[5] A. Wallraff *et al.*, Nature (London) **431**, 162 (2004).
[6] M. Steffen *et al.*, Phys. Rev. Lett. **97**, 050502 (2006).
[7] D. I. Schuster *et al.*, Nature (London) **445**, 515 (2007).
[8] O. Naaman and J. Aumentado, Phys. Rev. Lett. **96**, 100201 (2006).
[9] B. L. T. Plourde *et al.*, Phys. Rev. B **72**, 060506(R) (2005).
[10] J. M. Martinis *et al.*, Phys. Rev. Lett. **95**, 210503 (2005).
[11] R. W. Simmonds *et al.*, Phys. Rev. Lett. **93**, 077003 (2004).
[12] O. Astafiev *et al.*, Phys. Rev. Lett. **96**, 137001 (2006).
[13] D. J. Van Harlingen *et al.*, Phys. Rev. B **70**, 064517 (2004).
[14] F. C. Wellstood, C. Urbina, and J. Clarke, Appl. Phys. Lett. **85**, 5296 (2004).
[15] P. Dutta and P. M. Horn, Rev. Mod. Phys. **53**, 497 (1981); M. B. Weissman, Rev. Mod. Phys. **60**, 537 (1988).
[16] I. Martin, L. Bulaevskii, and A. Shnirman, Phys. Rev. Lett. **95**, 127002 (2005).
[17] A. Shnirman, G. Schön, I. Martin, and Y. Makhlin, Phys. Rev. Lett. **94**, 127002 (2005).
[18] R. H. Koch, D. P. DiVincenzo, and J. Clarke, Phys. Rev. Lett. **98**, 267003 (2007).
[19] A. M. Zagoskin, S. Ashhab, J. R. Johansson, and F. Nori, Phys. Rev. Lett. **97**, 077001 (2006); S. Ashhab, J. R. Johansson, and F. Nori, New J. Phys. **8**, 103 (2006).
[20] S. Oh *et al.*, Phys. Rev. B **74**, 100502(R) (2006).
[21] K. D. Osborn, J. A. Strong, A. J. Sirois, and R. W. Simmonds, arXiv:cond-mat/0703103.
[22] J. M. Raimond, M. Brune, and S. Haroche, Rev. Mod. Phys. **73**, 565 (2001).
[23] C. J. Hood *et al.*, Science **287**, 1447 (2000).
[24] C. Wang and R. Vyas, Phys. Rev. A **51**, 2516 (1995).
[25] T. P. Orlando and K. A. Delin, *Foundations of Applied Superconductivity* (Addison-Wesley, Reading, MA, 1991).
[26] U. Weiss, *Quantum Dissipative Systems* (World Scientific, Singapore, 1993).
[27] M. Lax, Phys. Rev. **129**, 2342 (1963).